Int. J. Electrochem. Sci., 6 **(2011)** 1045 - 1057

International Journal of
ELECTROCHEMICAL
SCIENCE
www.electrochemsci.org

Molecular Dynamics Simulation and Quantum Chemical Calculations for the Adsorption of some Thiosemicarbazone (TSC) Derivatives on Mild Steel

V. F. Ekpo[1], *P. C. Okafor*[1,*] , *U. J. Ekpe, E. E. Ebenso*[2]

[1]Corrosion and Electrochemistry Research Group, Department of Pure and Applied Chemistry, University of Calabar, P. M. B. 1115, Calabar, Nigeria.
[2] Department of Chemistry, North West University (Mafikeng Campus), Private Bag X2046, Mmabatho 2735, South Africa.
[*]E-mail: pcokafor@gmail.com

Received: 13 February 2011 / *Accepted:* 14 March 2011 / *Published:* 1 April 2011

The adsorption mechanism and inhibition performance of some thiosemicarbazone (TSC) derivatives [2-acetylpyridine thiosemicarbazone (2APTSC), 2-acetylpyridine-(4-methylthiosemicarbazone) (2AP4MTSC), 2-acetyl-pyridine-(4-phenylthiosemicarbazone) (2AP4PTSC), 2-acetylpyridine-(4-phenyl-iso-methylthiosemicarbazone) (2AP4PIMTSC) and 2-acetylpyridine-(4-phenyl-iso-ethylthiosemicarbazone) (2AP4PIETSC)] on mild steel at temperatures ranging from 298 K to 333 K have been studied using molecular dynamics (MD) simulation and quantum chemical computational methods. The results obtained revealed that these molecules could effectively adsorb on Fe (001) surface and the active adsorption sites of these molecules are the thiocarbonyl sulphur atoms, nitrogen atoms and special negatively charged carbon atoms. All the inhibitors studied had unique corrosion inhibition performance with AP4PIETSC showing the highest inhibition performance at lower temperature ranges of 298 K to 313 K and 2AP4PIETSC displaying the highest inhibition performance at higher temperature ranges of 323 K and 333 K. Physical adsorption mechanism was observed for all the inhibitors studied.

Keywords: Corrosion, mild steel, thiosemicarbazone derivatives, molecular dynamics

1. INTRODUCTION

Over the past decades, experimental methods have been used for corrosion inhibition studies and little knowledge on the interactions occurring between adsorbed molecules and the metal or alloy surface had been known. In addition, the microstructures and molecular properties of inhibitor

molecules could not be fully studied using experimental methods. In recent years, computational (theoretical) methods have been developed and these have been effective in studying the correlation of the inhibitor molecular properties and structure with inhibition efficiencies. Knowledge of the mechanism of corrosion inhibition now penetrates into the microscopic nano levels [1, 2].

Thiosemicarbazone (TSC) and its numerous derivatives are polar organic compounds containing the thiocarbonyl group and nitrogen atoms in their structures and have a high prospect as corrosion inhibitors [3, 4]. There have been numerous experimental investigations on the corrosion inhibitive capacities of TSC and its derivatives. Results obtained from these investigations reveal a strong dependence of the mechanism and inhibitor efficiency on the inhibitor structure, temperature as well as the concentration of the corrosive environment [4-11].

Using the computational methods, several factors and parameters are considered. These parameters referred to as quantum chemical parameters are special properties which are analyzed and used in the computational (theoretical) methods to study the corrosion inhibitive potentials of inhibitors. These can broadly be grouped into the energy, lattice, orbital and electrostatic parameters. Also included are the Fukui functions. From the 1970s, successful researches have been carried out in the field of corrosion inhibition using different computational (theoretical) methods [1, 2, 12-19]. However, literature search reveals that no complete computational study has been done on the inhibition ability of TSC and derivatives.

In the present work, molecular dynamics and quantum computational methods have been used to study the mechanism of corrosion inhibition of some thiosemicarbazone derivatives on mild steel. Also, the effects of corrosion inhibition process on the microstructure and quantum chemical properties of these compounds are discussed.

2. MATERIALS AND METHODS

The nomenclature, chemical formulae, molecular mass and structure of the thiosemicarbazone (TSC) derivatives used for this study are shown in Table 1 and Fig. 1.

Table 1. Names and molecular properties of TSC derivatives studied

S/N	Abbreviation	Name	Chemical formulae	Net mol. mass
1	2APTSC	2 acetyl pyridine thiosemicarbazone	C8H10N4S	**194.256**
2	2AP4MTSC	2 acetyl pyridine-(-4-methly thiosemicarbazone)	C9H12N4S	**208.283**
3	2AP4PTSC	2 acetyl pyridine-(-4-phenyl thiosemicarbazone)	C14H14N4S	**270.354**
4	2AP4PIMTSC	2 acetyl pyridine-(-4-phenyl isomethyl thiosemicarbazone)	C15H16N4S	**284.381**
5	2A4PIETSC	2 acetyl pyridine-(-4-phenyl isoethyl thiosemicarbazone)	C16H18N4S	**298.408**

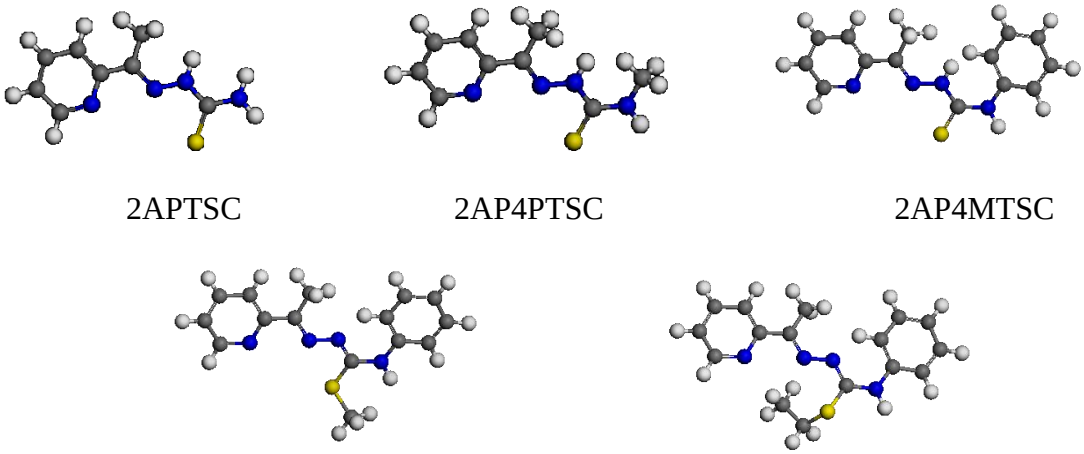

Figure 1.Structures of TSC derivatives studied

The inhibition properties of these compounds have been reported in previous work done in our laboratory [4, 6, 7, 9].

2.1. Molecular dynamics simulations

Molecular dynamic (MD) simulations were performed using the software, Material Studio (Version 4.0) from Accelyrs Inc. (San Diego, CA, USA). The MD calculation of the simulation of the interaction between the inhibitor molecules and the iron surface was carried out in a simulation box (2.009nm x 0.861 nm x 3.44 nm) with periodic boundary conditions to model a representative part of the interface devoid of any arbitrary boundary effects. The box consisted of a Fe slab and vacuum layer of height 2.81nm. The Fe crystal was cleaved along the (001) plane with the uppermost and the lowest layers released and the inner layers fixed. The MD simulations were performed under different temperatures (of 298, 303, 313, 323 and 333 K), NVT ensembled (with a time step of 0.1 fs) and simulation time of 5ps to observe the effect of changing temperatures on the inhibitor properties. A simulation time of 5ps was used to reduce the time spent for each run. The interaction energy $E_{Fe-inhibitor}$ of the Fe surface with the inhibitor was calculated according to equation (1) [2].

$$E_{Fe-inhibitor} = E_{complex} - E_{Fe} - E_{inhibitor} \quad (1)$$

With $E_{complex}$ being the total energy of the Fe crystal together with the adsorbed inhibitor molecule; E_{Fe} and $E_{inhibitor}$ being the total energy of the Fe crystal and Free inhibitor molecule, respectively. The binding energy is the negative value of the interaction energy.

$$E_{binding} = -E_{Fe\text{-}inhibitor} \quad (2)$$

For the whole simulation procedure, the force field CVFF (consistent valence force field) was used. This was primarily intended for studies of structure and binding energies, although it also predicted the vibrational frequencies and conformational energy reasonably well [2].

2.2. Quantum chemistry calculation

The quantum chemistry calculations were performed with Gaussian 03 programme using B3LYP method, 3 – 21 G(d) basis set to initially optimize the geometry structure of the five inhibitor molecules studied. The optimization was advanced with 6–31G(d) basic set and the frequency analysis was executed simultaneously, no imaginary frequency found, indicating that it was a minimum. The same method and basic set were used to research the structure and energy of the adsorbed molecule after MD simulation and the active site of the molecule was analysed. These procedures used for the MD simulation and quantum chemistry calculation were as used and designed by Xia *et al.*[2].

3. RESULTS AND DISCUSSIONS

3.1. Molecular dynamic simulation

The MD simulation was performed to study the adsorption behavior of the five (5) inhibiting molecules on the Fe (001) surface. The system reaches equilibrium only if both the temperature and energy reach a balance [2]. The adsorption configuration of the inhibitor molecules at initial (unabsorbed) and equilibrium (adsorbed) were studied (Fig 2 for 2APTSC at 298 K).

Table 2. Minimum distance between inhibitor molecules and Fe (001) surface

Inhibitor	**Minimum distance (nm)**					
	Initial	Equilibrium				
		298K	303K	313K	323K	333K
2APTSC	-	0.2718	0.2825	0.2941	0.2759	0.2836
2AP4MTSC	-	0.2942	0.2813	0.2653	0.2822	0.2785
2AP4PTSC	-	0.2641	0.2932	0.2833	0.2827	0.2853
2AP4PIMTSC	-	0.2858	0.2670	0.2625	0.2793	0.2716
2AP4PIETSC	-	0.2815	0.2751	0.2925	0.2898	0.2879

The minimum distances between the five inhibitor molecules and Fe surface at equilibrium for the various temperatures analyzed are as shown in Table 2. It is observed that the minimum distance of the inhibitor molecules from the Fe (001) surface lies between the range 0.2641and 0.2942 nm. According to the equilibrium configuration of the five inhibitors adsorbed on Fe (001) surface, it can be concluded that all the inhibitor molecules can be adsorbed on the Fe surface through the thiocarbonyl sulphur atom and nitrogen atoms with the inhibitor molecules being approximately planar

to the Fe surface. In this way, the exposed part of Fe surface can be reduced by the covering of the inhibitor molecules, consequently creating a barrier between the surface of the metal and the water. Furthermore, the non-polar part of the molecules spreading over the Fe surface prevents water molecule from getting in contact with the surface.

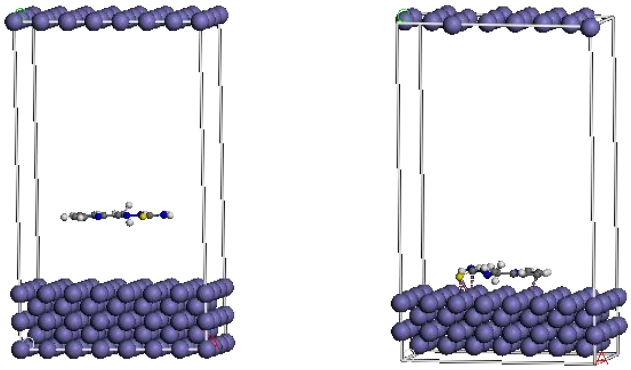

Initial (unadsorped) Equilibrium (adsorped)

Figure 2. Adsorption configuration of 2APTSC on iron surface at 298 K

Therefore, the corrosion inhibition is achieved by two factors. It can be inferred that the inhibitor molecules will form a waterproof film on the Fe surface after being added to the solution. This conclusion is in line with previous reports [6, 7].

Table 3. Interaction energy of inhibitors on Fe(001) surface (Kcal/mol)

Inhibitor	Temperature				
	298 K	303 K	313 K	323 K	333 K
2APTSC	-240.095	-234.389	-199.936	-214.203	-198.962
2AP4MTSC	-206.770	-227.015	-218.598	-231.689	-182.522
2AP4PTSC	-275.974	-245.101	-273.661	-245.897	-248.885
2AP4PIMTSC	-263.599	-271.064	-252.818	-277.082	-258.330
2AP4PIETSC	-289.208	-288.085	-303.379	-230.865	-256.411

The value of the interaction and binding energy of the inhibitors on Fe (001) surface at the various temperatures analyzed (298, 303, 313, 323 and 333 K) are listed in Table 3 and Table 4, respectively. From Table 3, it is seen that all the inhibitors have very low interaction energy. This indicates their ability to adsorb on the iron (Fe 001) surface. 2AP4PIETSC displayed the lowest interaction energy at lower temperatures of 298, 303 and 313 K while 2AP4PIMTSC displayed the lowest interaction energy at higher temperatures of 323 and 333 K. These two inhibitors therefore have the most effective interaction with iron surface at these temperatures, corresponding to their high binding energies.

Table 4. Binding energy of inhibitors on Fe (001) surface (Kcal/mol)

Inhibitor	Temperature				
	298K	303K	313K	323K	333K
2APTSC	240.095	234.389	199.936	214.203	198.962
2AP4MTSC	206.77	227.015	218.598	231.689	182.522
2AP4PTSC	275.974	245.101	273.661	245.897	248.885
2AP4PIMTSC	263.599	271.064	252.818	277.082	258.33
2AP4PIETSC	289.208	288.085	303.379	230.865	256.411

From Table 4, it is seen that all the inhibitors studied have a positive binding energy. The larger the value of the binding energy, the stronger the bonding between the inhibitor molecules and the iron surface, the easier the inhibitor molecules is adsorbed on the iron surface and thus the higher the inhibitor efficiency. At lower temperatures of 298, 303 and 313 K, 2AP4PIETSC has the highest binding energy of all the inhibitors studied and thus gives higher inhibition efficiency while at higher temperatures of 323 and 333K, 2AP4PIMTSC has the highest binding energy and thus gives higher inhibition efficiency.

Table 5. Trend of binding energies and inhibition efficiency of inhibitors

Temp (K)	Trend of binding energies and inhibition efficiency
298	2AP4PIETSC >2AP4PTSC > 2AP4PIMTSC > 2APTSC > 2AP4MTSC
303	2AP4PIETSC > 2AP4PIMTSC > 2AP4PTSC > 2APTSC > 2AP4MTSC >
313	2AP4PIETSC > 2AP4PTSC > 2AP4PIMTSC > 2AP4MTSC > 2APTSC
323	2AP4PIMTSC > 2AP4PTSC > 2AP4MTSC > 2APT4PIETISC > 2APTSC
333	2AP4PIMTSC > 2AP4PIETSC > 2AP4PTSC > 2APTSC > 2AP4MTSC

The trend of decreasing inhibitor binding energy and inhibition efficiency at the various temperatures are shown in Table 5. The trend of binding energy and inhibition efficiency as depicted by the inhibitors at 303K and 313K are in line with previous reports [6, 7, 9]. It is observed from Table 5, that apart from 2AP4PIETSC, which showed a higher binding energy and inhibition efficiency at lower temperatures of 298, 303 and 313 K, and 2AP4PIMTSC, which maintained the highest binding energy and inhibition efficiency at higher temperatures of 323K and 333K; the inhibitors showed varying binding energies and inhibitions efficiencies at the various temperatures. This according to

Okafor *et al.* [4] is contrary or does not follow the reports that physisorbed inhibitors of high molecular weight inhibit better than lower molecular weight inhibitors. This observation may be due to the changing orientation or structure of the inhibitor molecules at different temperatures, which at one point might favour or not favour a more effective interaction or binding of the inhibitor molecules on the Fe (001) surface.

3.2. Quantum chemistry calculation

Gaussian 03 program DFT B3LYP method was used to fully optimize the geometrical structure of the inhibitors. The optimized initial and equilibrium (adsorbed) structure for the TSC derivatives at 298 and 303 K are shown in Fig. 3.

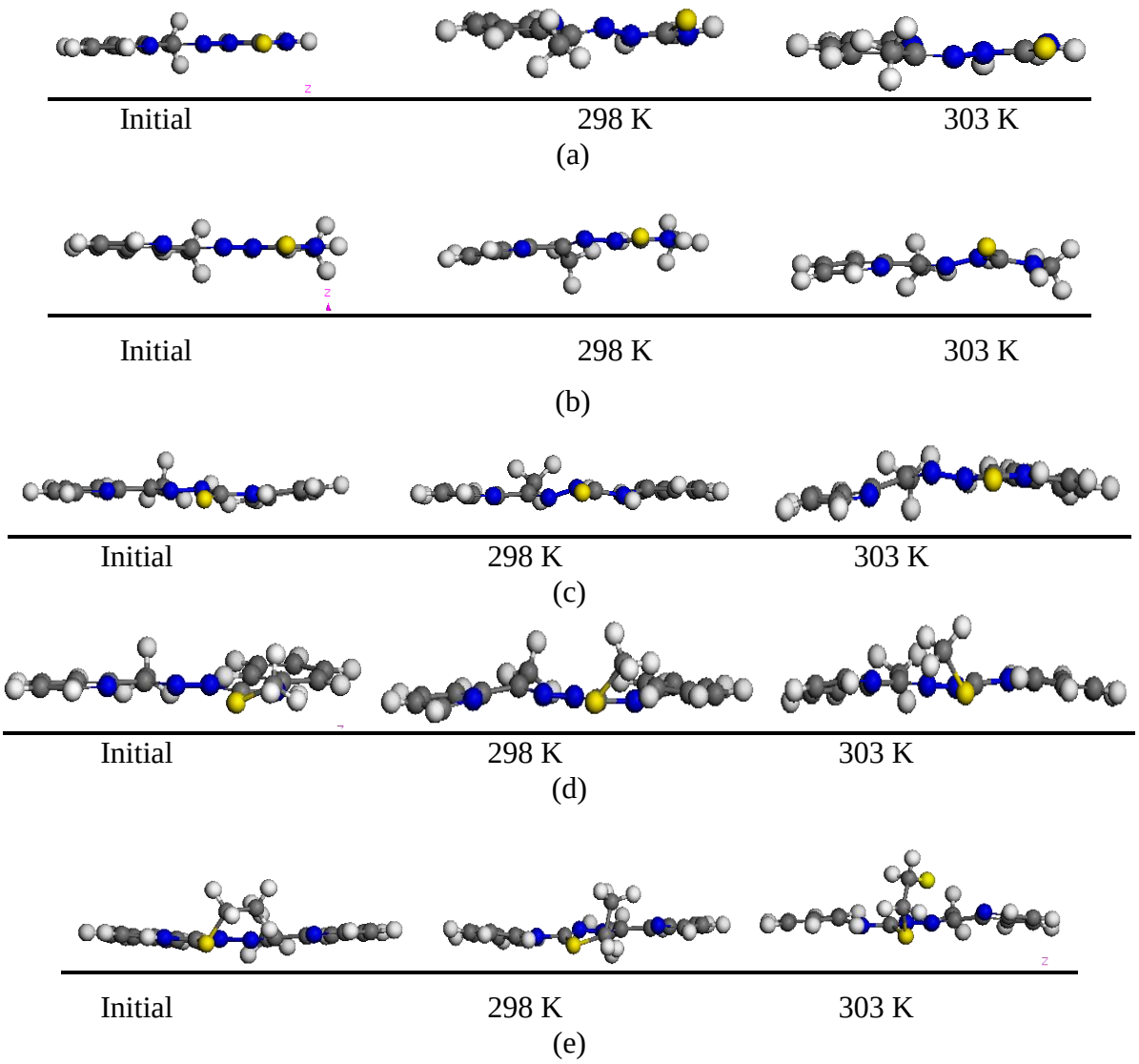

Figure 3. Optimized initial and equilibrium structures of inhibitor molecules for 2APTSC, 2AP4PTSC, 2AP4MTSC, 2AP4PIMTSC and 2AP4PIETSC

Table 6. Bond length analysis for the TSC derivatives at 298 K (in nm)

2APTSC			2AP4MTSC			2AP4PTSC			2AP4PIMTSC			2AP4PIETSC		
Bond	Initial (adsorbed)	Equil.	Bond	Initial (adsorbed)	Equil.	Bond	Initial (adsorbed)	Equil.	Bond	Initial (adsorbed)	Equil.	Bond	Initial (adsorbed)	Equil.
N_1 - C_2	0.1510	0.1313	N_2 - C_1	0.1509	0.1449	C_1-N_2	0.1513	0.1458	C_1-N_2	0.1514	0.1419	C_1-N_2	0.1514	0.1497
C_2 = S	0.1811	0.1654	N_2 - C_3	0.1510	0.1337	N_2-C_3	0.1515	0.1350	N_2-C_3	0.1512	0.1489	C_3-N_2	0.1513	0.1446
C_2 - N_3	0.1510	0.1273	C_3 = S	0.1810	0.1664	C_3=S	0.1811	0.1612	C_3-S_4	0.1809	0.1785	C_3-S_4	0.1812	0.1813
N_3 - N_4	0.1479	0.1435	C_3 - N_4	0.1510	0.1292	C_3-N_4	0.1511	0.1292	C_5-S_4	0.1809	0.1872	C_5-S_4	0.1812	0.1734
N_4 = C_5	0.1509	0.1241	N_5 - N_4	0.1480	0.1384	N_4-N_5	0.1409	0.1366	C_3=N_6	0.1508	0.1267	C_5-C_6	0.1541	0.1512
C_5 - C_6	0.1509	0.1487	N_5 = C_6	0.1509	0.1278	N_5=C_6	0.1509	0.1248	N_6-N_7	0.1480	0.1247	C_3=N_7	0.1509	0.1303
C_5 - C_7	0.1540	0.1690	C_6 - C_7	0.1539	0.1532	C_6-C_7	0.1540	0.1583	C_8=N_7	0.1509	0.1312	N_7-N_8	0.1478	0.1207
C_7 - N_8	0.1540	0.1337	C_6 - C_8	0.1539	0.1555	C_7=C_8	0.1540	0.1406	C_8-C_{15}	0.1540	0.1472	C_9=N_8	0.1508	0.1384
C_7 = C_{12}	0.1540	0.1376	C_8 - N_9	0.1512	0.1343	C_8 - C_9	0.1540	0.1359	C_8-C_9	0.1540	0.1519	C_9-C_{10}	0.1540	0.1614
N_8 = C_9	0.1512	0.1348	N_9 = C_{10}	0.1512	0.1347	C_9 = C_{10}	0.1540	0.1395	C_9=C_{10}	0.1540	0.1423	C_9-C_{11}	0.1540	0.1570
C_9 - C_{10}	0.1540	0.1370	C_{10} - C_{11}	0.1540	0.1405	C_{10} - C_{11}	0.1540	0.1447	C_9-N_{14}	0.1512	0.1360	C_{11}=C_{12}	0.1539	0.1437
C_{10} = C_{11}	0.1540	0.1414	C_{12} = C_{11}	0.1538	0.1360	C_{11} = N_{12}	0.1512	0.1313	C_{13}-N_{14}	0.1512	0.1343	C_{11}-N_{13}	0.1511	0.1303
C_{11} - C_{12}	0.1538	0.1416	C_{12} - C_{13}	0.1538	0.1437	N_{12}-C_7	0.1512	0.1368				C_{14}=N_{13}	0.1512	0.1396
			C_{13} = C_8	0.1539	0.1441	C_{13}-C_6	0.1539	0.1519						
S - Fe_1	-	0.2874	S – Fe	-	0.2942	S-Fe_1	-	0.2641	S_4-Fe_1	-	0.2835	S-Fe_1	-	0.2815
S - Fe_2	-	0.2718	S - Fe_2	-	0.3037	S-Fe_2	-	0.3525	S_4-Fe_2	-	0.2963	S-Fe_2	-	0.3080
N_1 – Fe	-	0.3076	N_2 – Fe	-	0.2998	N_2-Fe	-	0.3395	N_2-Fe	-	0.2858	N_2-Fe	-	0.3132
N_3 – Fe	-	0.3224	N_4 – Fe	-	0.2995	N_4-Fe	-	0.3233	N_6-Fe	-	0.3067	N_7-Fe	-	0.3162
N_4 – Fe	-	0.2988	N_5 – Fe	-	0.3023	N_5-Fe	-	0.2939	N_7-Fe	-	0.2876	N_8-Fe	-	0.2983
N_8 – Fe	-	0.2880	N_9 – Fe	-	0.3042	N_{12}-Fe	-	0.2961	N_{14}-Fe	-	0.3017	N_{13}-Fe	-	0.3093

Table 6 shows the bond length (nm) analysis of the initial and equilibrium structure (at 298 K) of the inhibitor molecules. This table shows that the bond lengths of individual bonds in the inhibitor molecules are affected by the adsorption process on the Fe (001) surface. The adsorption process affects the C = S (thiocarbonyl group) bond as a strain which is seen by the gradual variation at all the temperatures studied. The changing structure of these inhibitor molecules at the different temperatures also reveals an effect on bond angles by torsional effects. This observation is in line with the previous observations [2].

The active sites of the inhibitor molecule can be established by considering three influencing factors: natural atomic charge, distribution of frontier molecular orbital and Fukui functions or indices [2]. According to classical chemical theory, all chemical interactions are either by electrostatic or orbital interactions. Electrical charges in the molecule were obviously the driving force of electrostatic interactions. It is proven that local electric densities or charges are important in many chemical

reactions and physicochemical properties of compound [2]. Table 7 shows the natural atomic charges analysis for the inhibitor molecules at the various temperatures. From the atomic charges in Table 7, the total number of charge centers (negative and positive) of the TSC derivatives (Table 8) was generated. The negative charge centers could offer electrons to the Fe atoms to form coordinate bond while the positive charge centers can accept electrons from 3d orbitals of the Fe atom to form feedback bond, thus further strengthening the interaction of inhibitor and Fe surface. From Table, the corrosion inhibition performance can roughly be evaluated considering the total number of charge centers (positive and negative) in the inhibitor molecule. The high inhibition efficiency of 2AP4PIETSC and 2AP4PIMTSC can be inferred from their high number of charged centers of 12 and 10 respectively. This also relates to the binding energies of the molecules.

Table 7. Natural atomic charge analysis for the TSC molecules at 298 K

2APTSC			2AP4MTSC			2AP4PTSC			2AP4PIMTSC			2AP4PIETSC		
Atom	Initial charge (C)	Equil. charge (C)	Atom	Initial charge (C)	Equil. charge (C)	Atom	Initial charge (C)	Equil. charge (C)	Atom	Initial charge (C)	Equil. charge (C)	Atom	Initial charge (C)	Equil. charge (C)
N_1	-0.622	-0.622	C_1	-0.273	-0.278	C_1	+0.166	+0.136	C_1	+0.170	+0.150	C_1	+0.169	+0.146
C_2	+0.443	+0.417	N_2	-0.497	-0.511	N_2	-0.466	-0.519	N_2	-0.503	-0.496	N_2	-0.497	-0.491
S	-0.243	-0.260	C_3	+0.456	+0.441	C_3	+0.436	+0.428	C_3	+0.448	+0.479	C_3	+0.443	-0.466
N_3	-0.359	-0.341	S	-0.264	-0.272	S	-0.265	-0.279	S_4	-0.351	-0.355	S_4	+0.387	-0.440
N_4	-0.145	-0.183	N_4	-0.357	-0.348	N_4	-0.36	-0.358	C_5	-0.274	-0.266	C_2	-0.161	-0.146
C_5	+0.169	+0.195	N_5	-0.148	-0.176	N_5	-0.146	-0.183	N_6	-0.258	-0.240	C_6	-0.361	-0.366
C_6	-0.395	-0.360	C_6	+0.169	0.207	C_6	+0.170	+0.209	N_7	-0.142	-0.180	N_7	-0.261	-0.231
C_7	+0.194	+0.205	C_7	-0.397	-0.372	C_7	+0.192	+0.214	C_8	+0.171	+0.198	N_8	+0.261	-0.218
N_8	-0.268	-0.324	C_8	+0.193	+0.211	C_8	-0.115	-0.116	C_9	+0.188	+0.207	C_9	+0.161	+0.183
C_9	+0.061	+0.061	N_9	-0.269	-0.294	C_9	-0.098	-0.116	C_{10}	-0.116	-0.116	C_{10}	-0.380	-0.408
C_{10}	-0.103	-0.112	C_{10}	+0.059	+0.065	C_{10}	-0.105	-0.107	C_{11}	-0.100	-0.114	C_{11}	+0.186	+0.204
C_{11}	-0.096	-0.110	C_{11}	-0.104	-0.105	C_{11}	+0.059	+0.067	C_{12}	-0.106	-0.110	C_{12}	-0.108	-0.121
C_{12}	-0.110	-0.103	C_{12}	-0.098	-0.118	N_{12}	-0.269	-0.286	C_{13}	+0.056	+0.059	N_{13}	-0.325	-0.331
			C_{13}	-0.111	-0.104	N_{13}	-0.396	-0.368	N_{14}	-0.273	-0.293	C_{14}	+0.050	+0.044
									C_{15}	-0.389	-0.364			

Table 8. Charge centers (negative and positive) of the TSC derivatives (≥ ±0.150) (Initial values)

Inhibitor	Negative (-) charge centers	Positive (+) charge centers	Total numbers
2APTSC	N_1, N_3, C_6, N_8, S	C_2, C_5	7
2AP4MTSC	C_1, N_2, S, N_4, C_7, N_9	C_3, C_6	8
2AP4PTSC	N_2, S, N_4, N_{12}, C_{13}	C_1, C_3, C_6, C_7	9
2AP4PIMTSC	N_2, S_4, C_5, N_6, N_{14}, C_{15}	C_1, C_3, C_8, C_9	10
2AP4PIETSC	N_2, S_4, C_5, C_6, N_7, N_8, C_{10}, N_{13}	C_1, C_3, C_9, C_{11}	12

The trend is as follows: 2AP4PIETSC > 2AP4PIMTSC > 2AP4PTSC > 2AP4MTSC > 2APTSC

According to the frontier molecular orbital theory (FMO) of chemical reactivity, transition of electron is due to interaction between highest occupied molecular orbital (HOMO) and lowest unoccupied molecular orbital (LUMO) of reacting species. The energy of HOMO (E_{HOMO}) is directly related to ionization potential while the energy of LUMO (E_{LUMO}) is directly related to electron affinity. Higher values of E_{HOMO} indicate a tendency of the molecules to donate electrons to appropriate acceptor molecules with low energy or empty electron orbital (e.g. Fe with empty 3d orbitals).

Table 9. E_{HOMO} and E_{LUMO} values for the TSC derivatives

Inhibitor	Initial	Equilibrium				
		298 K	303 K	313 K	323 K	333 K
		E_{HOMO} (eV) values				
2APTSC	-4.335	-3.822	-4.495	-4.156	-3.973	-3.935
2AP4MTSC	-4.218	-3.992	-4.126	-3.984	-4.011	-4.337
2AP4PTSC	-4.444	-4.096	-4.443	-4.321	-4.267	-4.353
2AP4PIMTSC	-4.509	-4.179	-4.052	-3.852	-3.766	-3.834
2AP4PIETSC	-4.509	-3.598	-3.585	-3.717	-4.032	-3.694
		E_{LUMO} (eV) values				
2APTSC	-3.163	-2.638	-2.459	-2.487	-2.692	-2.74
2AP4MTSC	-3.106	-2.409	-2.272	-2.360	-2.442	-2.533
2AP4PTSC	-3.236	-2.429	-2.655	-2.503	-2.399	-2.493
2AP4PIMTSC	-3.022	-2.566	-2.467	-2.696	-2.432	-2.501
2AP4PIETSC	-3.242	-2.394	-2.413	-2.487	-2.313	-2.436

Table 10. Total dipole moment for inhibitor molecules

Inhibitor	Initial (μ, debye)	Equilibrium (μ, Debye)				
		298 K	303 K	313 K	323 K	333 K
2APTSC	6.6869	7.5907	6.0400	6.1673	7.4575	8.1714
2AP4MTSC	6.9108	7.4646	5.8479	6.7736	6.9751	6.2861
2AP4PTSC	6.0851	5.4337	6.4275	5.6570	6.5436	6.9688
2AP4PIMTSC	1.8289	2.1117	1.1525	2.3093	2.0226	1.5999
2AP4PIETSC	1.6639	1.0784	1.1399	1.8810	1.7643	1.6207

Table 11. Energy of deformability for inhibitor molecules

Inhibitor	Initial (KJ/mol)	Equilibrium (KJ/mol)				
		298 K	303 K	313 K	323 K	333 K
2APTSC	9595.771	9872.362	9855.378	9898.017	9905.067	9920.509
2AP4MTSC	10790.373	11108.441	11069.662	11070.909	11089.294	11040.801
2AP4PTSC	14543.979	15047.200	15096.32	15072.454	15035.067	15070.503
2AP4PIMTSC	15754.233	16255.597	16238.456	16234.862	16190.390	16251.219
2AP4PIETSC	16916.923	17427.240	17432.01	17479.327	17465.123	17399.699

The lower the values of E_{LUMO}, the stronger the electron accepting ability of the molecules. Table 9 shows the E_{HOMO} and E_{LUMO} values for the molecules at initial and at equilibrium at the various temperatures. Compared to the initial structure, the values of E_{HOMO} of the molecules increase and E_{LUMO} values also increase indicating that after adsorption on Fe (001) surface, the ability for electron donation increases while the ability for accepting electron decreases.

Table 12. Components of molecular orbitals (HOMO and LUMO) for inhibitor molecules at 298 K

2APTSC			2AP4MTSC			2AP4PTSC			2AP4PIMTSC			2AP4PIETSC		
Atom	Initial	Equil.	Atom	Initial charge (C)	Equil. charge (C)	Atom	Initial charge (C)	Equil. charge (C)	Atom	Initial charge (C)	Equil. charge (C)	Atom	Initial charge (C)	Equil. charge (C)
Fukui negative (-) indices (Mulliken values) f(-)														
C_1	-0.003	0.072	C_1	-0.003	0.006	C_1	-0.003	-0.002	C_1	0.002	-0.003	C_1	0.001	0.008
C_2	0.018	0.004	C_2	0.017	0.009	C_2	0.016	0.009	C_2	0.019	0.014	C_2	0.017	0.011
C_3	0.014	0.014	C_3	0.013	0.012	C_3	0.012	0.005	C_3	0.017	0.011	C_3	0.016	0.011
C_4	0.027	0.016	C_4	0.026	0.015	C_4	0.024	0.015	C_4	0.029	0.017	C_4	0.028	0.016
C_5	0.015	0.005	C_5	0.014	0.007	C_5	0.013	0.006	C_5	0.021	0.013	C_5	0.018	0.011
N_6	-0.001	-0.014	N_6	-0.001	-0.010	N_6	-0.002	-0.026	N_6	0.007	-0.008	N_6	0.000	-0.019
C_7	0.054	0.047	C_7	0.052	0.043	C_7	0.049	0.044	C_7	0.063	0.069	C_7	0.057	0.052
N_8	-0.069	-0.053	C_8	-0.016	-0.014	C_8	-0.013	-0.022	C_8	-0.008	-0.010	C_8	-0.011	0.021
N_9	0.010	0.015	N_9	-0.068	-0.047	N_9	-0.061	0.044	N_9	0.098	0.111	N_9	0.094	0.123
C_{10}	0.071	0.056	N_{10}	0.006	0.001	N_{10}	0.012	0.007	N_{10}	0.073	0.059	N_{10}	0.076	0.072
C_{11}	0.464	0.517	C_{11}	0.080	0.077	C_{11}	0.081	0.084	C_{11}	0.035	0.035	C_{11}	0.030	0.044
N_{12}	0.010	0.013	S_{12}	0.458	0.507	S_{12}	0.407	0.437	S_{12}	0.073	0.097	S_{12}	0.089	0.134
C_{13}	-0.016	-0.019	N_{13}	0.000	-0.013	N_{13}	-0.016	-0.016	C_{13}	-0.009	-0.012	C_{13}	-0.011	-0.041
			C_{14}	-0.012	-0.031	C_{14}	-0.003	0.001	N_{14}	0.020	0.025	C_{14}	-0.036	-0.021
									C_{15}	0.000	-0.001	N_{15}	0.019	0.009
												C_{16}	0.001	0.002
Fukui positive (+) indices (Mulliken values) f(+)														
C_1	0.027	0.045	C_1	0.028	0.044	C_1	0.022	0.038	C_1	0.02	0.017	C_1	0.018	0.023
C_2	0.022	0.003	C_2	0.022	0.016	C_2	0.022	0.013	C_2	0.02	0.021	C_2	0.020	0.017
C_3	0.034	0.081	C_3	0.034	0.033	C_3	0.029	0.022	C_3	0.025	0.016	C_3	0.024	0.017
C_4	0.054	0.044	C_4	0.054	0.057	C_4	0.049	0.055	C_4	0.044	0.037	C_4	0.042	0.034
C_5	0.025	0.025	C_5	0.025	0.019	C_5	0.023	0.013	C_5	0.02	0.015	C_5	0.019	0.012
N_6	0.056	0.078	N_6	0.057	0.046	N_6	0.049	0.038	N_6	0.042	0.028	N_6	0.034	0.025
C_7	0.054	0.052	C_7	0.053	0.066	C_7	0.054	0.063	C_7	0.050	0.070	C_7	0.049	0.067
N_8	0.090	0.083	C_8	-0.017	-0.030	C_8	-0.016	-0.030	C_8	-0.014	-0.025	C_8	-0.014	0.000
N_9	0.013	-0.001	N_9	0.092	0.096	N_9	0.082	0.070	N_9	0.058	0.044	C_9	0.047	0.048
C_{10}	0.003	-0.015	N_{10}	0.015	-0.001	N_{10}	0.008	0.003	N_{10}	0.012	0.012	N_{10}	0.014	0.010
C_{11}	0.138	0.120	C_{11}	0.005	-0.005	C_{11}	0.017	0.009	C_{11}	0.062	0.072	C_{11}	0.061	0.068
N_{12}	0.026	0.020	S_{12}	0.131	0.128	S_{12}	0.127	0.123	S_{12}	0.072	0.082	S_{12}	0.075	0.107
C_{13}	0.018	-0.018	N_{13}	0.022	0.017	N_{13}	0.009	0.003	C_{13}	-0.01	-0.009	C_{13}	-0.014	-0.022
			C_{14}	-0.011	-0.027	C_{14}	-0.001	0.002	N_{14}	0.02	0.018	C_{14}	-0.015	-0.016
									C_{15}	-0.007	-0.002	N_{15}	0.025	0.018
												N_{16}	-0.007	0.000

The total dipole moment (μ in Debye) and energy of deformation (E_{deform} in KJ/mol) are parameters characterizing the interaction between molecules [2]. The energy of deformability increases with the increase in μ, making the molecules easier to adsorb at the Fe (001) surface. The volume of inhibitor molecules also increases with the increase of μ. This increases the contact area between molecule and surface of iron and increasing the corrosion inhibition ability of inhibitors.

Tables 10 and 11 show the values of total dipole moment (μ) and energy of deformability (E_{deform}) for the inhibitors at the simulation temperatures studied. From the tables, 2AP4PIETSC and 2APS4PIMTSC have the highest E_{deform} but the lowest μ values. Generally, the E_{deform} and μ values for the inhibitors increases above their initial values for most of the temperatures studied. This adds to their high inhibition performance.

The main component of molecular HOMO and LUMO orbitals (i.e. the Fukui negative (-) and positive indices) are listed in Table 12. For all the inhibitors studied, the HOMO orbital plots are mainly constituted by the sulphur (S) atoms, some nitrogen atoms and carbon atoms indicating that they can provide electrons while the LUMO orbital plots are constituted by other nitrogen atoms and few carbon atoms indicating that they can accept electrons from the Fe surface to form feedback bonds. For detailed characterization of donor-acceptor interactions, frontier orbital electron densities on atoms (indicated by the Fukui functions) are used. For donor molecules, the HOMO density is critical to charge transfer (electrophilic electron density (f_r^N)). For these values, the sulphur atom in the thiocarbonyl group, the nitrogen atoms and special carbon atoms show higher values thus indicating the active sites of the inhibitor molecules.

4. CONCLUSIONS

Molecular dynamics (MD) simulation and quantum chemical computational methods were used to study the adsorption and inhibition ability of some thiosemicarbazone (TSC) derivatives [2-acetylpyridine thiosemicarbazone (2APTSC), 2-acetylpyridine-(4-methylthiosemicarbazone) (2AP4MTSC), 2-acetyl-pyridine-(4-phenylthiosemicarbazone) (2AP4PTSC), 2-acetylpyridine-(4-phenyl-iso-methylthiosemicarbazone) (2AP4PIMTSC) and 2-acetylpyridine-(4-phenyl-iso-ethylthiosemicarbazone) (2AP4PIETSC)] on mild steel at temperatures ranging from 298 to 333 K. Molecular dynamic data show that all the thiosemicarbazone derivatives studied can adsorb on Fe surface through the thiocarbonyl sulphur atom, nitrogen atoms and even carbon atoms with special negative charge centers. The molecules are adsorbed on an orientation relatively planar to the Fe surface. Quantum chemical calculation results confirm the active sites of the inhibitors to be the thiocarbonyl sulphur atom, nitrogen atoms and some carbon atoms. The adsorption mechanism obtained from the results reveal that the molecules can adsorb firmly on the Fe surface by donating electrons to Fe atoms and partially by accepting electrons from 3d orbitals of Fe atoms.

References

1. K.F. Khaled. *Electrochm. Acta*, 3(2008) 3484.
2. S. Xia, M. Qui, L.Yu, F. Lui and H. Zhao. *Corros. Sci., 50*(2008) 2021.
3. B. I. Ita and O. E. Offiong. *Mater. Chm. Phy. 48*(1997) 164.
4. P. C. Okafor, E. E. Ebenso and U. J. Ekpe. *Bull. of Chem. Soc. of Ethiopia, 18(2)* (2004) 181.
5. B. G. Ateya. *Electroanal. Chem. 76*(1976) 191.
6. U. J. Ekpe, U. J. Ibok, B. I. Ita, O. E. Offiong and E. E. Ebenso. *Mater. Chem. Phy. 40*(1995) 87.
7. E. E. Ebenso, U. J. Ekpe, B. I. Ita, O. E. Offiong and U. J. Ibok. *Mater. Chem. Phy. 60*(1999) 79.

8. B. I. Ita and O. E. Offiong. *Mater. Chem. Phy 70*(2001) 330.
9. P. C. Okafor, E. E. Oguzie, G. E. Iniama, M. E. Ikpi and U. J. Ekpe. *Global J. of Pure & App. Sci., 14(1)* (2008) 89.
10. P. C. Okafor, E. E. Ebenso, U. J. Ibok, U. J. Ekpe and M. I. Ikpi. *Trans SAEST, 38*(2003) 91.
11. U. J. Ekpe, P. C. Okafor, E. E. Ebenso, O. E. Offiong and B. I. Ita. *Bull. of Electrochem.* 17(3) (2001) 131.
12. J. Vosta and J. Eliaseck. *Corros. Sci. 11*(1971) 223.
13. J. M. Costa and J. M. Lluch. *Corros. Sci. 23*(1984) 929.
14. J. C. Zheng, W. L. Cao and Z. X. Wang. *J. Chinese Soc. for Corros. & Protection*, *6*(1986) 217.
15. D. X. Wang, S. Y. Li and Y. Yu. *Corros. Sci. 41*(1999) 1911.
16. E.E. Ebenso, D.A. Isabirye, N.O. Eddy, *Int. J. Mol. Sci.* 11 (2010) 2473.
17. E.E. Ebenso, T. Arslan, F. Kandemirli, N. Caner, I. Love, Int. J. Quantum Chem. 110 (2009) 1003.
18. N.O. Eddy, S.R. Stoyanov, E. E. Ebenso, *Int. J. Electrochem. Sci*. 5 (2010) 1127.
19. N.O. Eddy, E. E. Ebenso, *Int. J. Electrochem. Sci*. 5 (2010) 731.